High Field Cos-Theta FalconD-C Dipole Magnet Development at CERN

Arnaud Foussat, Nicola Sala, Sachin Gowrishankar, Juan Carlos Perez, Ariel Haziot, Carlos Fernandes, Lucio Fiscarelli, Mariusz Wozniak, Emmanuele Ravaioli, Oussama Id'Bahmane, Luca Gentini, Michael Guinchard, Oscar Sacristan De Frutosins, Elena Fernandez Mora, Ezio Todesco, Stefania Farinon, Alessandra Pampaloni, Massimo Sorbi, and Riccardo Umberto Valente

***Abstract*—The FalconD (Future Accelerator post-LHC Cos-θ Optimized Nb_3Sn Dipole magnet is part of the High Field Magnet (HFM) CERN programme. In collaboration with the Italian Institute for Nuclear Physics (INFN Genova and LASA Milano), CERN is developing a $\cos\theta$ dipole magnet beyond 12 T based on proven Nb_3Sn technology in the MQXF quadrupole used in the high-luminosity upgrade of the LHC. The magnet, with design aperture diameter of 50 mm, provides a bore field of 12 T for a 73 TeV center-of-mass energy scenario for the Future FCC-hh Circular Collider. The project has specific objectives to investigate cos-θ short magnet model design based on a two-layers coil with a wide high current cable. Moreover, the study of mechanical dipole structures based on aluminum shell with bladders and key (*B&K*) developed for the HL-LHC MQXF quadrupole will be presented as a baseline. The structure pre-loading system assembly baseline shall be tested on sub-scale mechanical mock ups at 77 K prior to building two single aperture 1.5 m long Nb_3Sn magnet models followed by a 2-in-1 dipole magnet assembly. In this paper, we provide an overview of the magnetic and structural design carried out at CERN on an increased aperture diameter variant supported by first preliminary winding trials and give insights of the project timeline. Some preliminary protection scheme assessment is presented as baseline to be tested. Following the cable winding outcomes and the mechanical properties measured, some alternative coil optimized magnetic cross-section is reported.**

***Index Terms*—High field magnet programme, future circular collider, high-field dipole, Nb_3Sn cos theta magnets, aluminum shell, bladder and keys structure.**

I. Introduction

THE Future Circular Collider FCC-hh is proposed as a successor of Large Hadron Collider (LHC) baseline with a 85 TeV energy center of mass to open the energy frontiers for new particles physics discovery [1]. The CERN High Field Magnet (HFM) programme is developing for FCC-hh a high field bending dipole superconducting magnet with operating bore field of 14 T and 1.9 K, with 20% load-line margin, based on niobium–tin technology [2]. One of the FCC optional scenario is to consider the double layer cos-θ dipoles topology aiming at 12 T operational field with a 25% load-line margin [3]: this has the advantage of a well-established coil layout with high field effectiveness [4], already proven as extended to 7-m-long magnets [5]. It can provide a 15% lower center of mass energy (73 TeV) alternative scenario with a potential cost reduction of 20%, mainly due to a 30% reduction in the use of Nb_3Sn cable.

The 12 T double layer cos-θ option has been first proposed in 2020 [6]–[10], by INFN. In 2021, a similar magnet layout was proposed at CERN [11], however with 15% smaller diameter strand, resulting in 0.5 T lower short sample field, although easier to wind on the 50 mm aperture. Recently, it has been decided to enhance synergies and common projects objective to gain efficiency and reduce risks (as it was done for the early integrated development team of the HL-LHC quadrupoles [12][13] in the US and at CERN). The winding tests of the INFN design, carried out with the final cable both at CERN and at ASG company premises under the helm of INFN-Genova in 2024–2025 have shown difficulties in the coil heads [14], namely protrusions gaps of several millimeters in the last turn of the inner layer requiring design adaptation of ends. For these reasons, a more conformal alternative solution with the same cable but with a 56 mm (12% larger) aperture has been proposed by CERN to be investigated.

In this paper, we present the development of this latter design variant, called Falcon D-C, covering the magnetic and the mechanical design. This includes the adapted bladder and key dipole structure that take benefit from the experience and features of the HL-LHC quadrupoles as shown in Fig. 1.

II. Cable Parameters and Coil Requirements

A. CERN FalconD Coil Design (FalconD-C)

The strand used is the same within the whole FalconD project, i.e. a 1-mm-diameter strand based on Restacked Rod Process (RRP) technology, with 162/169 layout. This strand was ordered for the EuroCirCol program in view of a 16 T dipole design, and therefore has a quite low content of copper (Cu/NonCu ratio of 0.9). It has a non-Cu critical current density of 1200 A/mm ^{2}

Received 22 July 2025; revised 22 September 2025; accepted 9 October 2025. Date of publication 3 November 2025; date of current version 13 November 2025. *(Corresponding author: Arnaud Foussat.)*

Arnaud Foussat, Nicola Sala, Sachin Gowrishankar, Juan Carlos Perez, Ariel Haziot, Carlos Fernandes, Lucio Fiscarelli, Mariusz Wozniak, Emmanuele Ravaioli, Oussama Id'Bahmane, Luca Gentini, Michael Guinchard, Oscar Sacristan De Frutosins, Elena Fernandez Mora, and Ezio Todesco are with CERN Organisation 1, place d'Esplanade, 1211 Geneva, Switzerland (e-mail: Arnaud.foussat@cern.ch).

Stefania Farinon and Alessandra Pampaloni are with INFN-Sezione di Genova, I-16146 Genoa, Italy (e-mail: stefania.farinon@ge.infn.it).

Massimo Sorbi and Riccardo Umberto Valente are with INFN LASA Via Fratelli Cervi, I-20054 Milan, Italy (e-mail: massimo.sorbi@mi.infn.it).

Color versions of one or more figures in this article are available at https://doi.org/10.1109/TASC.2025.3628537.

Digital Object Identifier 10.1109/TASC.2025.3628537

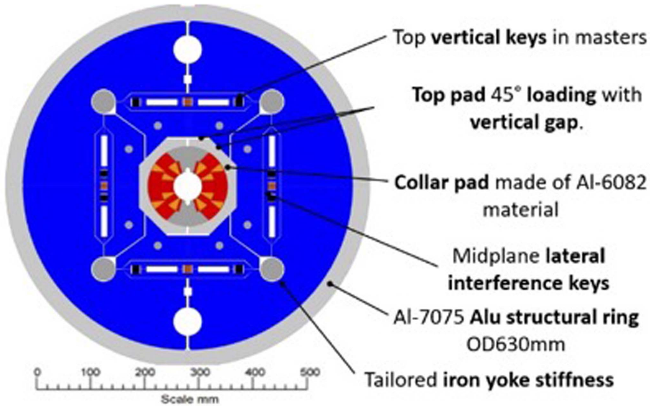

Fig. 1. Cross section view of the FalconD-C mechanical model.

TABLE I
RRP 162/169 STRAND SPECIFICATIONS AND CABLE PARAMETERS

Parameter	Value	Unit
Strand diameter	1.0	mm
Cu/NonCu	0.9±0.1	adim.
RRR	> 100	adim.
Cable bare width (before/after HT*)	21.0 / 21.4	mm
Cable bare mid-thickness (before/after HT)	1.81 / 1.89	mm
Cable I_c (12 T, 1.9 K)	> 58	kA
Non cu - J_c (16 T, 4.2 K)	> 1200	$\mathrm{A\,mm^{-2}}$
Non cu - J_c (12 T, 4.2 K)	> 2800	$\mathrm{A\,mm^{-2}}$
Cable S-2 glass insulation thickness	0.15	mm
Cable SS core thickness	25	µm
Cabling J_c degradation	< 5	%
*Heat Treatment		

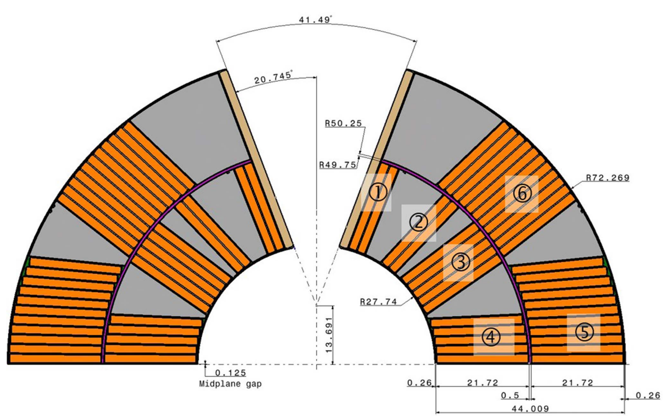

Fig. 2. FalconD-C 6-blocks coil cross section with a 56 mm aperture.

at 16 T and 4.22 K. The proposed Rutherford keystone cable is composed of 40 Nb_3 Sn strands whose properties are summarized in Table I.

The FalconD-C dipole coil section is composed of 36 turns, as shown in Fig. 2, and provides 12 T with 24% loadline margin at 1.9 K. A summary of the main parameters, and the comparison to the FalconD and to the previous 12 T 'robust' dipole, based on the MQXF cable with 40 strands and 0.85 mm diameter strand, is given in Table II. The FalconD designs have the advantage of a larger coil current density margin, since they

TABLE II
FALCOND MAGNET MAIN PARAMETERS COMPARISON

	FalconD	FalconD-C	12 T 'robust'
Aperture (mm)	50	56	50
Cable width (mm)	21.4	21.4	18.14
Nominal field (T)	12.0	12.0	12.0
Nominal peak field (T)	12.5	12.3	12.4
Nominal current (kA)	20.2	21.2	17.7
Loadline margin (%)	24.4	24.3	16.2
Equivalent coil width (mm)	37.4	35.7	29.8
Coil efficiency (T/A/mm)	0.00076	0.00075	0.00080
$J_o(A/mm^2)$	425	446	502
Number of turns	36	36	37
Bore midplane stress (MPa)	64	75	75
Stored energy (MJ/m)	0.55	0.56	0.45
Differential inductance $\mathrm{mH/m}$	2.23	3.1	2.3
Multipoles b_3, b_5, b_7 (10^{-4} Units)	0.3, -5.3, 12.6	6 ,-1.6, 1.6	N-A

make use of a 30% larger coil width. The current density is between 450 and 500 A/mm^2 in all cases, and the analytical estimate of the midplane stress in the bore [2] is between 64 and 75 MPa, i.e. well smaller than the 90 MPa obtained for the 11 T dipole developed for HL-LHC. This is thanks to the smaller aperture, and to the lower current density. The FalconD-C design allows an easier coil end, with very similar cable quantity and margin, at the price of a 10 MPa increase of midplane stress.

III. PRELIMINARY WINDING ENDS DESIGN

A. Coil End Geometry Optimization Method

The three-dimensional (3-D) coil ends geometry has been designed within the integrated ROXIE magnetic design using the differential geometry method [15]. One of the key optimisation conditions to be fulfilled using the genetic algorithm, especially when using wide cable, is to minimize the cable strain energy in each coil block as shown in section IV in order to limit any local geometrical instability like strand pop-outs. This objective can be expressed as the form of cable strain energy (1):

$$E = \frac{1}{2}\int_0^s \left[f_\tau \cdot \tau^2(s) + f_{k_g} \cdot \kappa_g^2(s) + f_{k_n} \cdot \kappa_n^2(s)\right] ds \quad (1)$$

where s is the cable length. The contributing curvature parameters denote the torsion τ, the normal curvature κ_n (or easy-way bend), and the geodesic curvature κ_g (the hard-way bend). f_τ, f_{k_n}, and f_{k_g} represent the respective flexural rigidities of the cable which are usually unknown for a given layout.

In order to quantify the magnitude for the flexural rigidity of the new cable in normal direction compared to some known used cables, we measured the proportional stiffness K_n coefficient ($\mathrm{N \cdot mm^{-1}}$) in the small displacement range using a 4-point bending standard test (ASTM D-6272). This rigidity defined as $E_\theta . I_{xx}/L_{eq}$ where E_θ is the azimuthal Young modulus, I_{xx} the moment of inertia about soft axis, and L_{eq} is the equivalent tested length, was measured at 44 $\mathrm{N \cdot mm^{-1}}$ that is, 43% greater than for the 18 mm wide MQXF cable. About the hard-way axis, as the moment of inertia of cable is increased by 97% with respect to the known MQXF cable, it confirms relative larger observed geodesic flexural rigidity.

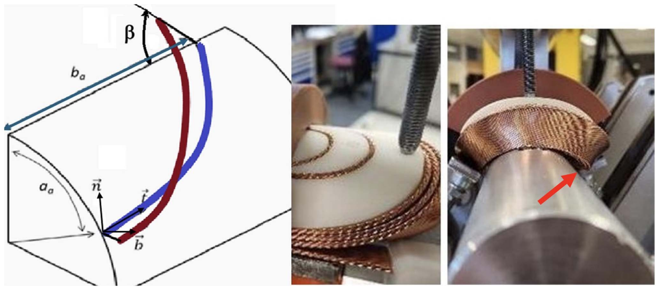

Fig. 3. (Left) Geometrical optimization parameters in coil block ends, (Right) Copper cable winding trial on 50-mm mandrel with residual radial gap.

B. Inner Layer Blocks Winding Trial

To support the design calculation a series of comparative inner layer winding trials were carried out first 50 mm diameter mandrel (i) with a dummy copper cable, then (ii) with $\mathrm{Nb_3Sn}$ cable with a set of pre-optimized 3D printed PLA plastic end spacers. This test revealed some strand pop-outs instability in the central pole block with highest β angle (see Fig. 3), and build-up of radial protrusion gaps between the mid plane 4^{th} block (see Fig. 2) and the mandrel up to 3–4 mm. This total gap was canceled out during the trial with the 56 mm diameter mandrel.

C. Mid-Plane Block Inclination Angle Test

Those last results were complemented by testing on the mid-plane coil block (azimuthal angle 0–180°) the single turn 'developable' differential geometry to confirm preferential natural inclination β angle. This test revealed that the use of the wide cable with a 50 mm aperture is prone to large hard bending and torsion amount responsible of the turn geometrical deviations. This issue could be only mitigated by diluting torsion along a longer conductor path, i.e increasing end length z_o to 240 mm to keep strain energy below critical empirical limits and reduce radial gap below 1-2mm. This elongated ends layout results in about 5 times less hard bending strain as confirmed by calculation with an optimized mid plane β angle of 60°.

Following both inner layer winding on 50 mm and mid-plane block winding trial outcomes in the 50 and 56 mm apertures, CERN decided to explore this latter enlarged aperture design. This is characterized by the conventional ends design geomtry as a more outcome of differential geometry optimization process in order to minimize further risks of geometrical deviations in the subsequent coils fabrication steps.

IV. Magnetic Analysis

The two-layers dipole coil magnetic section with 6-blocks and 56 mm aperture as shown in Fig. 4 follows similar architecture as the dipoles of LHC or HL-LHC 11 T R&D [16]. The coil section design uses related empirical heat treatment expansion coefficients of $\mathrm{Nb_3Sn}$ cable respectively in width and thickness at 2% and 4.5%, based on the HL-LHC main inner triplet quadrupole (MQXF) experience. The magnetic optimization and allowed b_n multipoles minimization was performed using the integrated BEM-FEM Roxie package [17] including ferromagnetic yoke

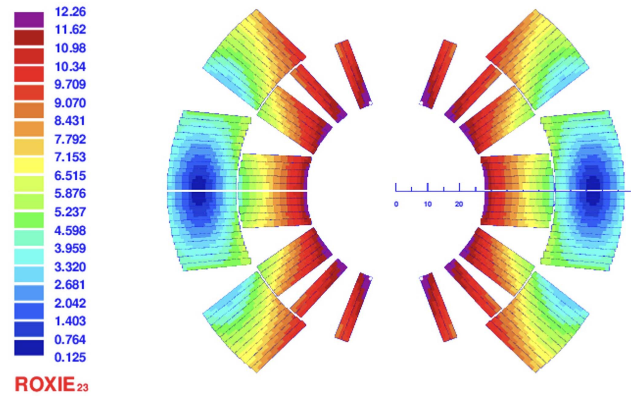

Fig. 4. Magnetic flux density contour of FalconD-C at nominal 21.2 kA current.

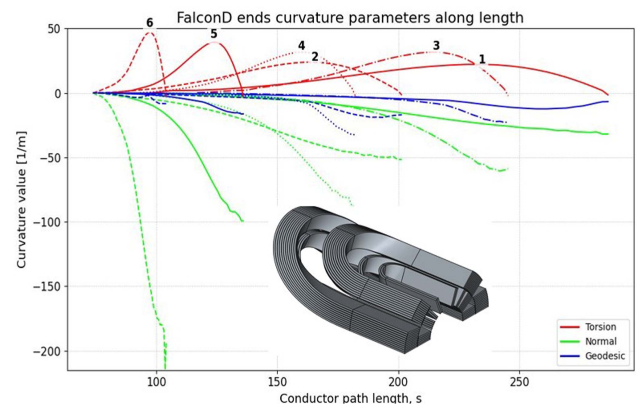

Fig. 5. Optimisation outcomes over Normal τ_n, Geodesic τ_g curvatures and Torsion T content along each block 1 to 6.

geometry over a reference radius of 37 mm. The coil ends were also optimized to minimize integrated multipole content.

Roxie package allows differential geometry optimization [18] to minimize the mechanical cable stress using the global multi-variable EXTREM routine. Some empirical inter-turn built-up gaps were assumed from 0.35 mm to 0.5 mm at the innermost conductors tips in conjunction with the set of following design parameters to be optimized:

- The inclination angle β of innermost turn blocks on mandrel as a key parameter of elastic ribbon differential geometry developed in Darboux frame,
- The order of ellipticity $\lambda = b_o/a_o$ and super ellipse n-order,
- Four spline-fitting torsion parameters as local adjustment,
- relative Z-position of block coils.

For every block geometry, the edge of regression ϑ criteria is checked, indicating any intersection of generatrix while bending the ribbon-like cable. The minimization of both curvature and torsional cable strains was performed on each coil end block, resulting in successive peaks variation within 40% along the cable paths as shown in Fig. 5. The new Roxie Application Programming Interface (API) allows to run multi-optimization and display parameters domain space around each selected optimum value as illustrated in the example of the torsion τ_n amount as function of H-order and β angle in Fig 6.

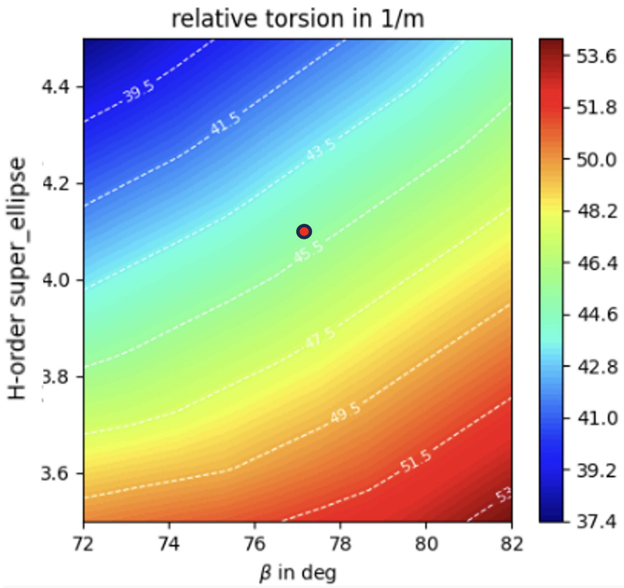

Fig. 6. Response surface around nominal optimum value of torsion curvature τ_n for the block 1 as function of β angle and H-order.

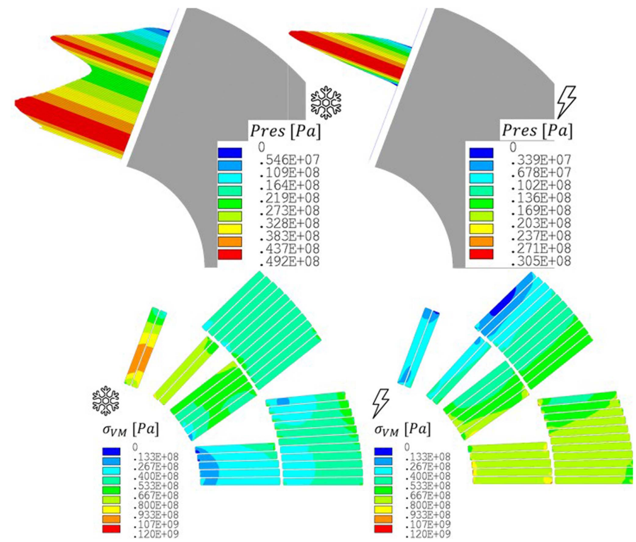

Fig. 7. Von Mises (VM) coil stress contour and both poles contact pressure profile in FalconD coil at cold and under 12 T Lorentz loads.

V. Mechanical Design

The magnet mechanical shell based-structure provides a rigid support around the coils whilst maintaining at cold during all operating steps a maximum conductor displacement of 60 μ m in mid plane corresponding to the maximum 120 MPa Von Mises stress criteria. A minimum contact pressure at pole during energisation ($\simeq$ 5 MPa) is targeted by design. The equivalent stress level in the coil stays below design limits for the brittle Nb_3 Sn material, respectively both at RT assembly under 120 MPa and 150 MPa at cold power operation.

A. Structure Description

The mechanical magnet preloading system relies on Aluminium shell with bladders and keys technology developed by US-LARP in the early HQ model [19] and more recently in the production of HL-LHC series MQXF quadrupole magnets [20]–[21]. The novelty of FalconD-C structure lies in the adaptation of the B&K to the cos-θ dipole geometry with a detachable shimmed pole to allow better contorl of applied azimuthal stress. This is adjusted through the use of horizontal and vertical (H,V) keys optimally positioned, acting distinctly with an optimized interference ratio of 3:1 respectively set at 0.15 mm and 0.45 mm per quadrant. Similarly to the 11 T HL-LHC R&D coil, a potted copper-alloy oxide dispersion strengthened (ODS) wedge is used in the outer layer with a common load plate to match the azimuthal size of both layers. The structure should guarantee effective support against the horizontal electromagnetic applied force of Fx = 3.77 MN/m in mid plane quadrant and the vertical ones at −1.90 MN/m at cold. A loading sequence at room temperature was proposed inflating alternatively both sets of bladders V, H with incremental pressure of 10 bars or equivalent 0.01 mm opening gap with a maximum pressure capacity of 4.5 MPa. The contact surface boundary of the top iron pads (see Fig 1) to the coil aluminum collar are designed with gaps so that the pole loading plane is well-controlled without overloading the mid plane.

B. Mechanical Sub-Scale Short Mock-Up

For the purpose of fast turnaround mechanical structure test platform at cold, a first sub-scale mock-up named LMK1 has been devised using existing 600 mm long 11 T HL-LHC coil cut sections. It utilizes an existing outer 7075-T6 aluminium alloy QXF shell, 29 mm thick with an outer diameter of 614 mm (32 mm thick, 630 mm outer diameter on FalconD-C magnet). The design was then focusing on dimensioning yoke pads components to find an optimum loading sequence for an equivalent scaled FalconD-C 12 T Lorentz loads.

C. 2D FE Modelling

A detailed 2D structural ANSYS FEM analysis was carried out on both the mock up and final FalconD coil section to predimension and to explore the parameters space of the magnet assembly. The stress levels in coils were assessed both in LMK1 mock up and FalconD dipole coil including the overshoot gap of 0.2 mm for inserting the keys. The optimized loading sequence was evaluated, keeping a ratio of 3:1 in the horizontal to vertical applied keys interferences with steps of 50 micrometers which offers possibility to define the nominal shimming and to keep safe coil peak stress at maximum 70 MPa below the design limit at room temperature (see Fig 7). The incremental key gap of 0.05 mm corresponds to a bladder pressure increase of 32 bars and a contact pressure of 12 MPa at the poles. At the end of magnet pre-load assembly, a springback is present of maximum −15 MPa (see Fig. 8) on the coil pole stress and about −40 MPa in the Aluminum shell which provided final coil stress level at RT below −55 MPa.

At 1.9 K, and in any operational power condition, the coil peak stress remains below 80 MPa and pole contact average stresses below design value of 5 MPa.

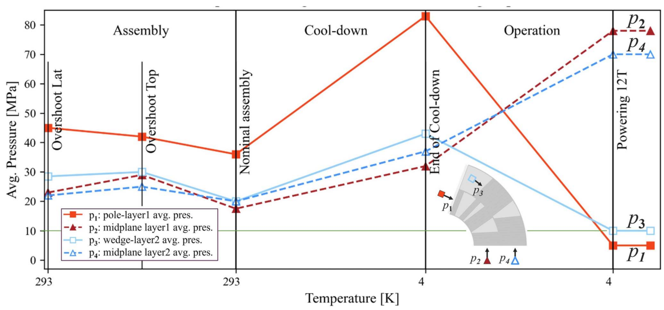

Fig. 8. FalconD-C coil mid plane and pole average VM stress in assembly steps, cool down and power condition.

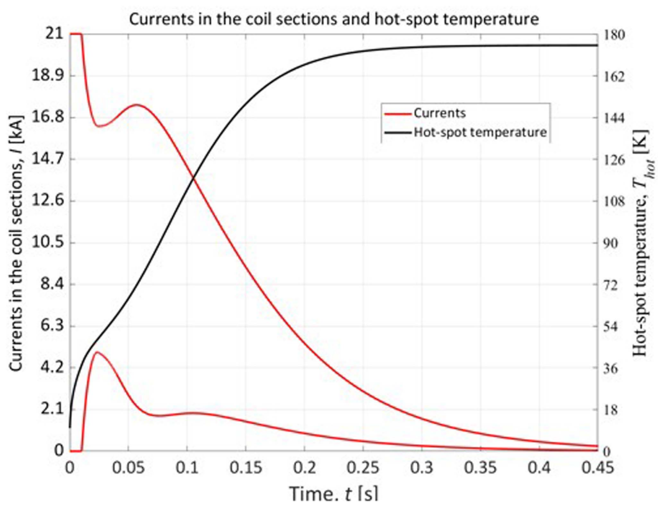

Fig. 9. Hot-spot temperature, main magnet and ESC coils currents for ESC based protection triggered at 10 ms for a FalconD-C 5 m model.

VI. Magnet Protection Scheme

The protection design targets for impregnated coils an adiabatic hot spot temperature lower than 300 K. The conventional quench heater protection [22] given the low fraction of copper stabilizer (Cu/NonCu:0.9) of FalconD cable would be less effective, reaching an estimated hotspot including AC losses of 350 K with a 10 ms detection time. With the FalconD dipole stored energy density, 2.5 times larger than in LHC main dipole at $89\mathrm{MJ\,m^{-3}}$, the minimal estimated available protection time margin with respect to temperature design limit for the FalconD coil is 50 ms [23].

Although the FalconD 2 m short model will be tested in combination of a baseline external dump energy resistor, an alternative standalone self magnet protection is required for longer accelerator-type magnet. The novel Energy Shift with Coupling (ESC) method was proposed as an R&D point of interest to be preliminary assessed on a 5-m long model and has shown a peak hot spot temperature closer to 175 K using the STEAM-LEDET package [25] [26] as shown in Fig 9. The concept shall be tested for validation at CERN on one of next short models [24] to protect magnet during a discharge by using close magnetically coupled auxiliary insulated copper coil. The method eliminates advantageously the need for direct electrical or physical contact with main superconducting coil. Once the quench is detected, a rapid triggered current shift imposes high magnetic field change on the superconductor, hence accelerating the normal state transition.

VII. Conclusion

As part of HFM program, the CERN magnetic and mechanical design analysis of new FalconD-C dipole coil and structure layout based on 56-mm aperture with the use of wide high current $\mathrm{Nb_3Sn}$ cable was presented. A first 12 T magnet model, expected to be assembled and cold tested at CERN by the end 2026, relies on the aluminum shell-based bladders and keys preload optimized system taking lessons learnt from HL-LHC. To experimentally study the novel dipole structure behavior at cold, some sub-scale mechanical mock up is planned to be built by end 2025 to validate proof of principle based on existing $\mathrm{Nb_3Sn}$ 11 T coil material section. The relative preliminary 2D mechanical analysis was performed to assess the structure and coil behavior during pre-loading, cool-down and excitation at nominal current. The peak Von Mises stress in the coil section during assembly and cold powering remain within respective set limits of 120 MPa and 150 MPa. ESC (Energy Shift with Coupling) quench protection method will be demonstrated for the first time on a cos theta dipole model. A 3D magnetic analysis was performed to minimize the harmonics content in the coils ends region and to optimize the end spacers differential geometry for fast prototyping and allow a first winding trial by end 2025. Further three-dimensional structural analysis is planned to investigate further the stress in the coils ends and to optimize the axial loading system.

Acknowledgment

The authors would like to acknowledge Matthias Bonora for the useful support during the Roxie magnetic modelling.

References

[1] A. Abada et al., “FCC-hh: The hadron collider,” *Eur. Phys. J. Spec. Top.*, vol. 228, pp. 755–1107, 2019, doi: 10.1140/epjst/e2019-900087-0.
[2] E. Todesco et al., “Status and perspectives in high field superconducting magnets for particle accelerators,” in *Proc. Appl. Supercond. Conf. (ASC 2024)*, Aug. 2025.
[3] S. Farinon et al., “Advancements in $\mathrm{Nb_3Sn}$ 12 T cos-theta dipole development for next-generation accelerators: The INFN-CERN collaboration on the FalconD project,” *IEEE Trans. Appl. Supercond.*, vol. 35, no. 5, Aug. 2025, Art. no. 4001905.
[4] J. van Nugteren et al., “Idealized coil cross sections with minimized conductor area for high field dipoles,” *IEEE Trans. Appl. Supercond.*, vol. 28, no. 3, Apr. 2018, Art. no. 4901505, doi: 10.1109/TASC.2018.2795536.
[5] G. Vallone et al., “Assembly of a mechanical model of MQXFB, the 7.2-m-Long low- β quadrupole for the high-luminosity LHC upgrade,” *IEEE Trans. Appl. Supercond.*, vol. 29, no. 5, Aug. 2019, Art. no. 4000605.
[6] R. U. Valente et al., “Update on the electromagnetic design of the $\mathrm{Nb_3Sn}$ cos-theta dipole model for FCC-hh,” *IEEE Trans. Appl. Supercond.*, vol. 32, no. 4, Jun. 2022, Art. no. 4001005.
[7] A. Pampaloni et al., “Preliminary design of the $\mathrm{Nb_3Sn}$ $cos\theta$ short model for the FCC,” *IEEE Trans. Appl. Supercond.*, vol. 31, no. 5, Aug. 2021, Art. no. 4900905.
[8] R. U. Valente et al., “Study of superconducting magnetization effects and 3D electromagnetic analysis of the $\mathrm{Nb_3Sn}$ $cos\theta$ short model for FCC,” *IEEE Trans. Appl. Supercond.*, vol. 31, no. 5, Aug. 2021, Art. no. 4002205.

[9] A. Pampaloni et al., “Mechanical design of FalconD, a Nb_3Sn $Cos\theta$ short model dipole for the FCC,” *IEEE Trans. Appl. Supercond.*, vol. 32, no. 6, Sep. 2022, Art. no. 4000605.

[10] F. Levi et al., “Updates on the mechanical design of FalconD, a Nb_3Sn $Cos\theta$ short model dipole for FCC-hh,” *IEEE Trans. Appl. Supercond.*, vol. 33, no. 5, Aug. 2023, Art. no. 4000805.

[11] M. Masci, D. Perini, and L. Baudin, “Mechanical design of the 12 T superconducting dipole. An accelerator-fit, Nb_3Sn double aperture magnet,” in *Proc. 15th Int. Part. Accel. Conf.*, May 2024, Art. no. WEPS63.

[12] S. Izquierdo Bermudez et al., “Mechanical analysis of the Nb_3Sn 11 t dipole short models for the high luminosity large hadron collider,” *Supercond. Sci. Technol.*, vol. 32, no. 8, 2018, doi: 10.1088/1361-6668/ab1f39.

[13] F. Savary et al., “Progress on the development of the Nb_3Sn 11T dipole for the high luminosity upgrade of LHC,” *IEEE Trans. Appl. Supercond.*, vol. 27, no. 4, Jun. 2017, Art. no. 4003505.

[14] R. U. Valente et al., “Winding challenges and solutions in the INFN falcon dipole project,” *IEEE Trans. Appl. Supercond.*, vol. 36, no. 3, May 2026, Art. no. 4000705.

[15] B. Bauer, “Modelling, analysis and computational methods for a one-dimensional formulation of developable elastic ribbons,” Doctoral dissertation, Fraunhofer Inst. Ind. Math. (ITWM), Verlag, Dec. 2022.

[16] G. Ambrosio et al., “Magnetic design of the fermilab 11 T Nb_3Sn short dipole model,” *IEEE Trans. Appl. Supercond.*, vol. 10, no. 1, pp. 322–325, Mar. 2000.

[17] S. Russenschuck, “ROXIE-A computer code for the integrated design of accelerator magnets,” *CERN*, Geneva, Switzerland, CERN-LHC-Proj. Rep. 276, 1999.

[18] B. Auchmann and S. Russenschuck, “Coil end design for superconducting magnets applying differential geometry methods,” *IEEE Trans. Magn.*, vol. 40, no. 2, pp. 1208–1211, Mar. 2004.

[19] S. Caspi et al., “The use of pressurized bladders for stress control of superconducting magnets,” *IEEE Trans. Appl. Supercond.*, vol. 11, no. 1, pp. 2272–2275, Mar. 2001.

[20] P. Ferracin et al., “Development of MQXF: The Nb_3Sn Low-β quadrupole for the HiLumi LHC,” *IEEE Trans. Appl. Supercond.*, vol. 26, no. 4, Jun. 2016, Art. no. 4000207.

[21] H. Pan et al., “Mechanical design studies of the MQXF long model quadrupole for the HiLumi LHC,” *IEEE Trans. Appl. Supercond.*, vol. 27, no. 4, Jun. 2017, Art. no. 4004105.

[22] S. I. Bermudez et al., “Overview of the quench heater performance for MQXF, the Nb_3Sn low-β quadrupole for the high luminosity LHC,” *IEEE Trans. Appl. Supercond.*, vol. 28, no. 4, Jun. 2018, Art. no. 4008406.

[23] L. Bottura et al., “WAMSDO: Workshop on accelerator magnet superconductors design and optimization,” *CERN, Geneva, Switzerland, Tech. Rep. CERN–2013–006,* Nov. 2013 .

[24] E. Ravaioli, A. Verweij, and M. Wozniak, “Energy shift with coupling (ESC): A new quench protection method,” *Supercond. Sci. Technol.*, vol. 38, 2025, Art. no. 035009.

[25] “STEAM FEM CERN package for simulation of transient effects in accelerator magnets”. [Online]. Available: https://indico.cern.ch/event/1161448

[26] E. Ravaioli et al., “Lumped-Element Dynamic Electro-Thermal model of a superconducting magnet,” *Cryogenics*, vol. 80, no. Part 3, pp. 346–356, Dec. 2016.